CB note 349

Analysis of the reaction $\bar{p}p \to K^+K^-\pi^0$ at 900 and at 1642 MeV/c

I. Uman * *Ludwig-Maximilians-Universität München, Am Coulombwall 1, D-85748 Garching, Germany*

The antiproton-proton annihilation into $K^+K^-\pi^0$ has been studied at incident beam momenta of 900 and 1642 MeV/c with the Crystal Barrel detector at LEAR. A partial wave analysis has been carried out. At lower momenta a $J^{PC} = 1^{--}$ state which is probably a superposition of the vectors $\phi(1680)$ and $\rho(1700)$ has been observed at a mass of 1700 ± 8 MeV ($\Gamma = 143 \pm 24$ MeV). There is a strong production of $f_0(1500)$ at both momenta. $f_2'(1525)$ is also clearly distinguished by its interference with $f_0(1500)$. Another state at $M = 1750 \pm 13$ MeV ($\Gamma = 148 \pm 34$ MeV) with spin 0 preferred over spin 1,2 and 3 has been observed at higher momentum. This resonance is most likely the $f_0(1710)$.

1. Introduction

Preliminary results in $\bar{p}p \to K^+K^-\pi^0$ at 900 and at 1642 MeV/c which were part of my Ph.D. work [1] were shown at the LEAP '00 conference [2].

This report gives additional information on many points that came up in the continuous discussion with Wolfgang Duennweber on the forthcoming publication. While checking the stability of my preliminary fits I found out that the resonance parameters came out to close to the start parameters in some cases due to overfitting. To avoid unphysical results I have reduced the number of free parameters by subsequent approximations. Another improvement concerns the resonance amplitude. In the present analysis I use mass-dependent width in the denominator of the Breit-Wigner amplitude and centrifugal barrier penetration factors in the nominator and denominator, as became custom in CB publications. The new method will be described below. Qualitatively, most of the old results are confirmed, but the relative resonance strengths are different. As will be shown, absolute cross sections for the present annihilation channels can be obtained by normalization to known cross sections for the $\pi^+\pi^-$ and K^+K^- annihilation channels.

The evidence for the $f_0(1710)$ at 1642 MeV/c is now stronger since its interferences with the $(K\pi^0)$ resonances are included in the new approach. The status of this scalar resonance and of neighbouring spin 1 and 2 resonances is much clearer in the present Particle Data Book than 5 years ago. The full model space of accessible PDG resonances is investigated in the present analysis.

2. Data Selection and Event Reconstruction

The data samples consist of 18.8 and 12.4×10^6 *2-prong* triggers at 900 and 1642 MeV/c, respectively. The trigger combines the start signal of the beam entrance counters and a veto scintillator behind the target with the information on the charge multiplicity from the SVX and the JDC.

The software that has been used for reconstruction was the standard version of the one that has been used for data at rest updated with new photon energy calibration [3],[4] and new resistive wire length scaling [5]. The data selection and event reconstruction is identical to the one fully described in [1].

A charge multiplicity 2 or 3 in the SVX detector and two in layers 9 and 10 of the JDC was required for the *2-prong* trigger. $K^+K^-\pi^0$ data are selected imposing the following cuts:

- Exactly two long tracks, one positive and one negative, with a minimum number of 10

*Now at Northwestern University, Illinois, USA

JDC hits per track, irrespective of whether additional short tracks ($<$ 10 hits) are present. Both tracks must begin within the inner three JDC layers. In addition the $\chi^2/d.o.f$ of the helix fit must be less than 1.5. Because of the Lorentz boost no cuts on the outer layers were performed in order to increase the coverage of the solid angle.

- Exactly two photons in the calorimeter which are not pointed by a charged track were demanded. Every photon corresponds to an electromagnetic shower in a group of adjacent crystals. A cut on the E_1/E_9 ratio of the energy of the central crystal relative to the sum with the neighboring crystal was used in order to reject clusters produced by electronic noise.

  A minimum deposited energy of 1 MeV for a crystal and at least an energy of 13 MeV for the central crystal was required. Two software algorithms, Dolby-C [6] and TAXI [7], were used to discard those events where one of the two photon is associated to a splitoff or induced by the interaction of a charged track. The former routine is more specific for finding electromagnetic splitoffs and is based on the topological distribution of a pair of PEDs and of the 'asymmetry-opening angle plot'. The latter technique extends the possible area of hadronic splitoffs in the neighborhood of a matched PED with a different clustering algorithm. Events with exactly 2 golden gammas are accepted, irrespective of whether there are additional split-offs in the event. Such split-offs are ignored in the event reconstruction.

- An additional cut for tracks converging to a unique vertex point has been performed. For annihilation in flight the antiproton can annihilate at any point within the target region along the beam axis. To improve the quality of the data the direction cosines of the photons are calculated with respect to these vertex coordinates.

- The π^0 signal was identified as coming from a π^0 decay into two photons. The two-photon invariant mass is calculated for the only possible combination and a cut on $145 < m_{\gamma\gamma} < 155$ MeV is performed.

- Energy/momentum balance was imposed under the hypothesis that the two charged tracks are kaons. The energy and momentum distributions peak at the nominal antiproton beam momentum (LEAR) and the total energy in the laboratory frame. Different enrichment regions that correspond to different final states are visible in the two dimensional scatter plots (see fig. 1) showing the total momentum versus the total energy.

By these cuts the initial sample is reduced to 60687 and 15240 events at 900 and 1642 MeV/c respectively. Each of the remaining events is required satisfying a 5C kinematic fit with confidence level (CL)$>$ 10%. The main backgrounds of events fitting $\pi^+\pi^-\gamma\gamma$ and $\pi^+\pi^-\pi^0$ are rejected requiring a CL$<$ 1%. Further checks on the separation of $\pi^+\pi^-\pi^0$ from $K^+K^-\pi^0$ are made using the differential energy loss dE/dx, plotted as a function of the momentum of the charged mesons (Bethe-Bloch formula [12]) (see fig. 2).

Monte Carlo simulation were done to estimate feed-through contributions from 4-body final state reactions which may remain in our final event selection. It was found that the contributions of $K^+K^-\pi^0\pi^0$ and $K^{+-}K_L\pi^{-+}\pi^0$, with two missing photons and a non-interacting K_L, respectively, is 3 orders of magnitude below that of the present channel. Hence the background from these channels is totally negligible.

The background cuts rejecting $\pi^+\pi^-\gamma\gamma$ and $\pi^+\pi^-\pi^0$ have negligible effect in the Dalitz plot at 900 MeV/c reducing the statistics at 900 MeV/c by only 0.2%. At higher momentum instead about 10% of good $K^+K^-\pi^0$ events are rejected. These events are mainly distributed in the extreme bottom left of the Dalitz plots at 1642 MeV/c, where both kaons are fast and of equal momentum. The cut affects the acceptance of K^+K^- resonances which have a mass where the $K^*(890)$ cross, that is at $\sim$ 2050 MeV. Back-

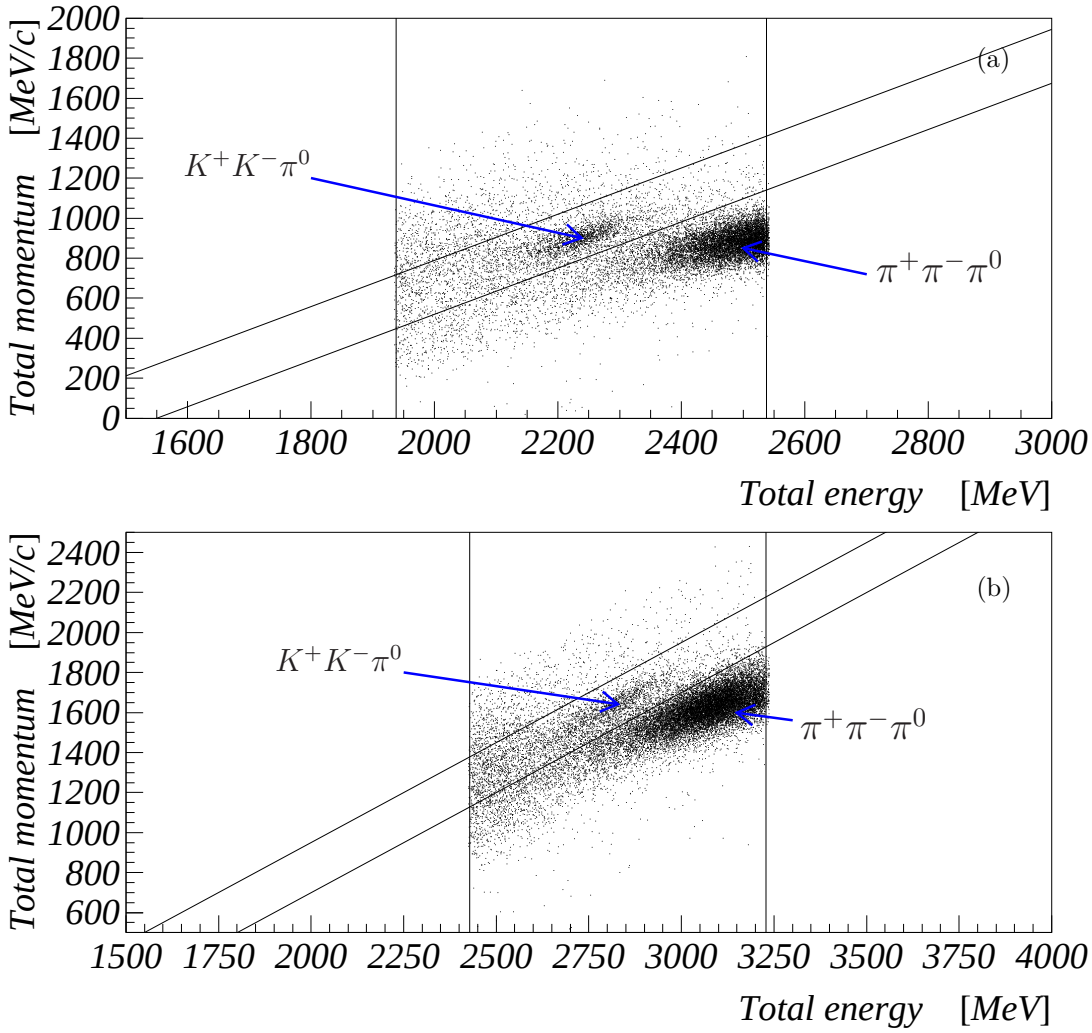

Figure 1. Energy/momentum balance was imposed under the hypothesis that the two charged tracks are kaons at 900 MeV/c (a) and at 1642 MeV/c (b) incoming $\bar{p}$ momentum. The $K^+K^-\pi^0$ states are distinguishable from the the most populated one which corresponds to the final $\pi^+\pi^-\pi^0$ state. The accepted events are between the lines drawn.

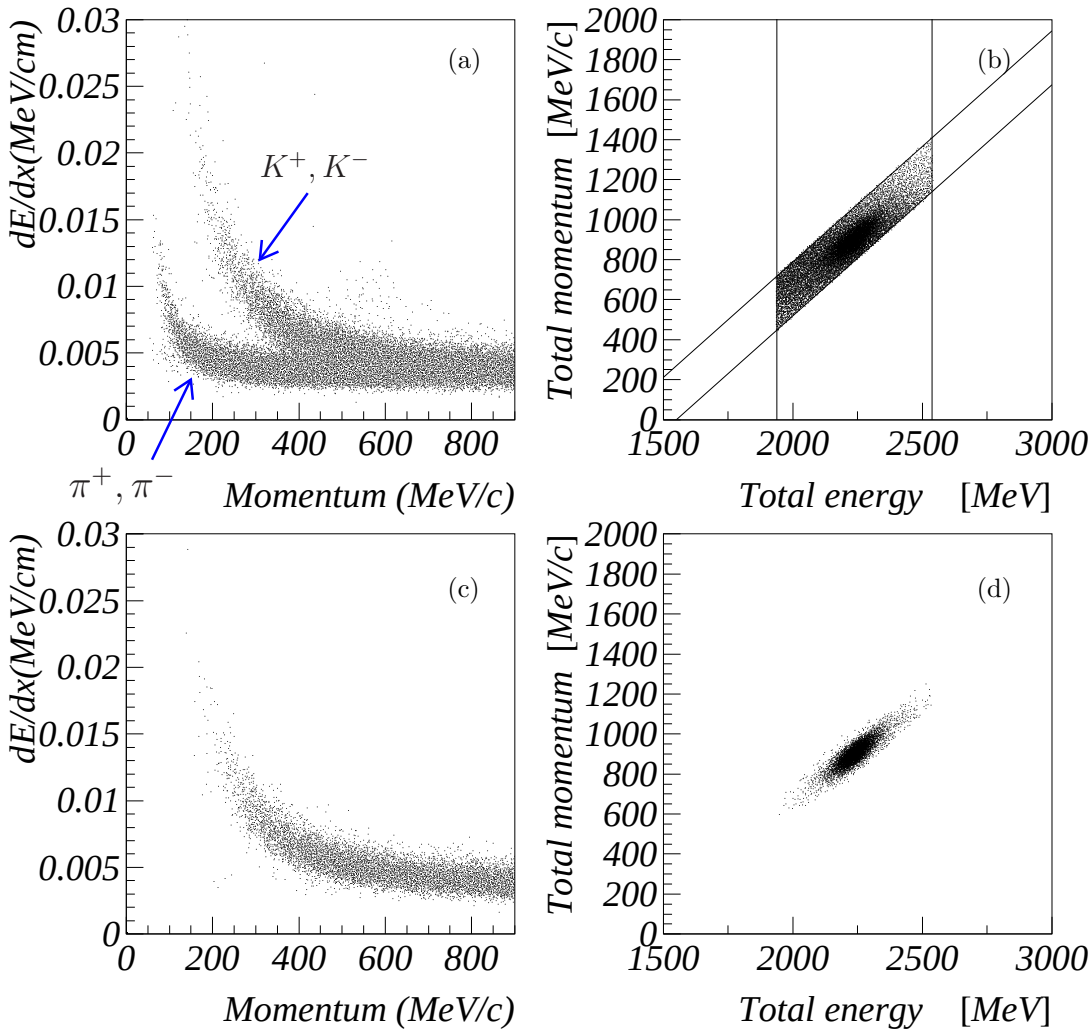

Figure 2. The differential energy loss versus the momentum which follows the Bethe-Bloch formula ([12]) of the charged mesons at 900 MeV/c (a) shows that both $K^+K^-\pi^0$ and $\pi^+\pi^-\pi^0$ states are still present after energy/momentum balance (b) and fig. 1,(a). $\pi^+\pi^-\pi^0$ final states are removed after a kinematic fit (c),(d).

ground from $\pi^+\pi^-\pi^0$ is irrelevant up to an invariant K^+K^--mass of ~ 2 GeV.

After all cuts 15036 and 4271 events at 900 and at 1642 MeV/c, respectively are left for the final analysis.

A full Monte Carlo simulation of the detector based on the GEANT program [8] with a new updated version of the FLUKA shower simulation was used. This version has a more realistic extension to low kaon momenta (below 1 GeV/c) with respect to other standard packages used in high energy physics. In addition, as in the real data, a flat $\bar{p}p$ annihilation z-vertex distribution has been simulated. 1 million and 5×10^5 phase space distributed events for $K^+K^-\pi^0$ were generated at 900 and at 1642 MeV/c respectively and submitted to the same cuts as the real events. These show an efficiency for reconstruction and selection of $K^+K^-\pi^0$ events of about 8.2% and 7.6% at 900 and at 1642 MeV/c, respectively.

The Dalitz plots and the projections are shown in fig. 3.

Consider first the Dalitz Plot at 900 MeV/c. The most evident structures are vertical and horizontal $K^{*\pm}(892)$ bands. Close to the boundary the narrow diagonal band of the $\phi(1020)$ is visible. Three further enrichment regions are at $M(K^+K^-) \sim 1300$ MeV, at ~ 1500 and at ~ 1660 MeV. The first two are likely to be identified with the $f_2(1270)$, the $f_0(1500)$. The latter could be the $f_0(1710)$. However resonances which decay into K^+K^- have isospin 0 or 1 and C-parity equivalent to P-parity. Therefore the peak at 1660 MeV can be also associated to $a_2(1700)$, $\phi(1680)$, $\rho(1700)$ and $\rho_3(1690)$. The $a_2(1320)$, $f_2'(1525)$ could also be present.

The same structures are also evident at an incoming antiproton momentum of 1642 MeV/c. However here the data shows a peak around $\sim$ 1740 MeV, while at 900 MeV/c this is at ~ 1660 MeV, as can be clearly seen from the mass projections (fig. 3,(c) and (f)).

3. Analysis Method

The analysis assumes that in the transition to the $K^+K^-\pi^0$ final state intermediate states with resonances between any pair of final state meson can be formed.

Due to the many initial angular states of the initial $\bar{p}p$ system a full description of the transition to the final $K^+K^-\pi^0$ state is not possible with the present statistics. We are interested in the decay process which contains mainly the information of the spin of the resonance. In the initial fits the production angular distribution which is sensitive to the partial waves involved in the production process is not considered. In the final fits the dependence on production angle theta is parameterized by $(cos\theta)^n$ terms (see below). The high number of initial states justifies this simplification. This formalism is described in earlier CB papers [9], [10].

We outline the method taking the channel $\bar{p}p \rightarrow f_2(1270)\pi^0$ as an example. The initial $\bar{p}p$ system has helicity ± 1 or 0. The resonance $f_2(1270)$ is produced at an angle (θ, ϕ) with respect to the beam direction and π^0 is the recoiling meson. The transition amplitude is invariant under a Lorentz transformation to the center of mass system of the resonance. A sequence of operations, rotations by θ, ϕ and Lorentz transformation to the center of mass of the resonance is performed. A second rotation by $-\phi, -\theta$ cancels the D rotation matrices which would otherwise be needed for the first rotation. These operations allow to describe the decay of the resonance by spherical harmonics $Y_J^\lambda(\alpha, \beta)$. Here α and β (see fig. 4) are the polar and azimuthal decay angles, J is the spin of the resonance and λ is the component of the spin along the original beam axis that we choose as the quantization axis.

In the process $\bar{p}p \rightarrow f_2(1270)$ the $f_2(1270)$ can have the $\lambda = \pm 2, \pm 1$ or 0.

In general we parameterize the decay of every resonance by amplitudes

$$A_J^\lambda = G_\lambda e^{i\delta_\lambda} F_J(q) \frac{Y_J^\lambda(\alpha, \beta)}{m_0^2 - s - i m_0 \Gamma(m)}, \qquad (1)$$

The denominator is that for the relativistic Breit Wigner with mass dependent width,

$$\Gamma(m) = \Gamma_0 \left(\frac{m_0}{m} \frac{q}{q_0} \frac{F_J^2(q)}{F_J^2(q_0)} \right), \quad m = \sqrt{s}. \qquad (2)$$

Here $F_J(q)$ are the standard Blatt-Weisskopf barrier factors for the resonance break-up momen-

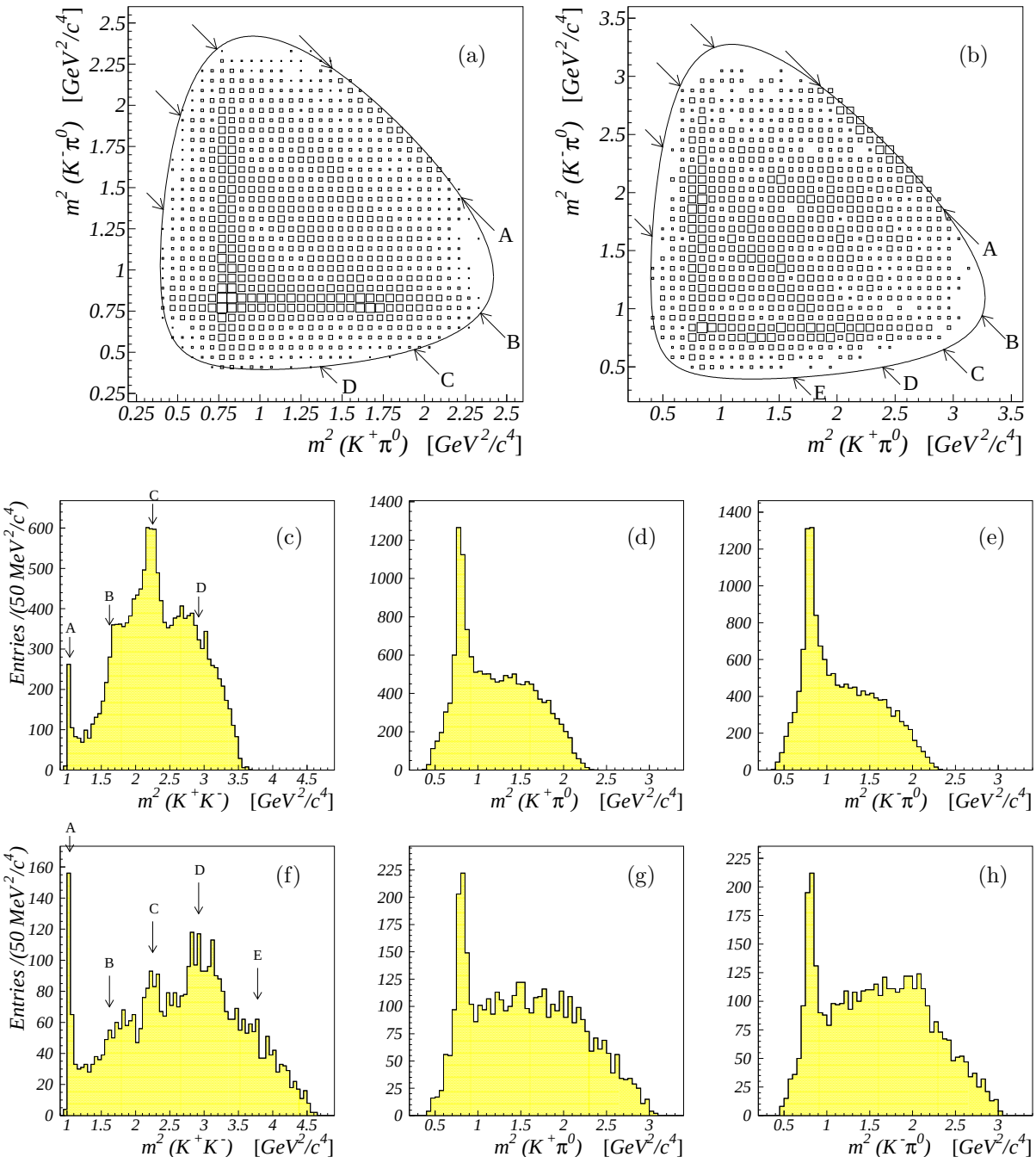

Figure 3. Dalitz plot of the final sample of 15036 (a) and 4271 (b) events from $\bar{p}p \to K^+K^-\pi^0$ at 900 MeV/c (a) and 1642/c MeV (b) $\bar{p}$ momentum. The data are not acceptance corrected and not symmetrized and binned with cell size 60 MeV$^2/c^4$ × 60 MeV$^2/c^4$ (a) and 85 MeV$^2/c^4$ × 85 MeV$^2/c^4$ (b). The symbol area is proportional to the number of events. The arrows indicate the positions of m(K^+K^-)= 1020(A),1275(B),1500(C),1710(D) and 1945(E) MeV/c^2. (c)-(e) Projections at 900 MeV/c, (f)-(h) projections at 1642 MeV/c.

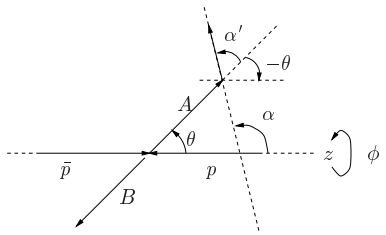

Figure 4. Definition of angles in the canonical formalism.

tum q (subscripts 0 denote values at the resonance mass, m_0). G_λ and δ_λ are the magnitude and the phase of the complex coupling constant. The cross section and hence the values of G_λ and δ_λ are the same for positive and negative values of λ, while there is a separate coupling constant and phase for $\lambda = 0$ and every positive value.

In the case of the $f_2(1270)$ and the $a_2(1320)$ the dominant alternative decay channels are taken into account in the mass dependent width in the fashion described in Ref. [9]:

$$\begin{aligned}\Gamma(m) &= \Gamma_0[(\rho_i(m)/\rho_i(m_0))B_L(q,q_0)_i^2\ \gamma_i^2 + \\ &+ (\rho_{KK}(m)/\rho_{KK}(m_o))B_L(q,q_0)_{KK}^2\ \gamma_{KK}^2]\end{aligned}$$

where ρ_i designates the phase space factor $q_i/2m$ and $B_L(q,q_0)_i$ the ratio of the barrier factor at break-up momentum q(m) over that at q_0. Here i designates the dominant $\pi\pi$ or $\rho\pi$ decay channels of the f_2 or a_2, respectively, where L=2. The decay probabilities are normalized as $\gamma_i^2+\gamma_{KK}^2 = 1$.

Resonance yields are obtained by integrating $\sum_\lambda |A_J^\lambda|^2$ over phase space. The total intensity is obtained by integrating over phase space the squared magnitude of the sum of the amplitudes of all channels. It is normalized to the known cross sections of 2-body channels, as outlined in Section 6, to yield the total cross section. The total intensity, unlike the resonance yields, includes interferences of different resonances. Since the experiment covers the full range of production angles, the total cross section and the relative resonance yields are integrals over the full angular range.

For a given λ, interferences between all channels may occur. Since there are many initial partial waves the interference between e.g. the $f_2(1270)$ with another resonance, say $K_1(890)$ may only be partially coherent. For this case the intensity w is given by the equation

$$\begin{aligned}w(m,m') = &\ \textstyle\sum_\lambda[|A_{f_2}^\lambda(m)|^2 + |A_{K_1}^\lambda(m')|^2 + \\ &+2c_\lambda \Re(A_{f_2}^\lambda(m) A_{K_1}^{\lambda *}(m')] \qquad (3)\end{aligned}$$

where c_λ is constrained to lie within the range 0 (no coherence) and ± 1 (full coherence). For states with different λ, it is assumed [9,10] that their interferences average to zero since the spectator meson K or π^0 has spin zero and since all resonance decay angles are integrated over. This assumption was tested for the prominent resonances in the fits below. No interference of this type could be found that fulfills the likelihood criteria specified below.

We define the log-likelihood $ln\mathcal{L}$ as follows:

$$ln\mathcal{L} = (\sum_{j=1}^{N} lnw_j) - Nln(\sum_{i=1}^{M} w_i) \qquad (4)$$

where N is the number of data events, M is the number of Monte Carlo events. The free parameters of the fit $(G_\lambda, \delta_\lambda, c_\lambda)$ are optimized in order to give the most negative value of the log-likelihood. With this definition, and for a fixed set of parameters, a reduction of $ln\mathcal{L}$ by 0.5 is statistically significant and corresponds to one standard deviation.

Although we ignore most features of the production process, to simulate in an approximate way the θ dependence amplitudes are multiplied by a factor of

$$F(\theta) = 1 + r_1 cos\theta + r_2 cos^2\theta + ... \qquad (5)$$

The production parameters r_1, r_2, ... are fitted separately from the decay parameters $G_\lambda, \delta_\lambda$ and c_λ. Small modifications of the resonance yields, resulting from refitting the production parameters in a few cases, are included in the final results. A possible dependence of the production parameters on the spin projection λ was also

studied. This type of λ dependence is not significant in most cases. It was found that the resulting effects on the resonance yields are small enough to be included in the errors (see below).

After every optimization a χ^2 test is performed. The experimental Dalitz plot is divided in bins with different sizes but with an equal number of contents: 1024 bins with approximately 16 entries for the Dalitz plot at 900 MeV/c and with ~ 4 entries at 1642 MeV/c. The χ^2 in a bin is calculated using an adaptation of the standard Pearson χ^2 (see [11]):

$$\chi^2 = \sum_i \frac{(n_i - f_i m_i)^2}{f_i(n_i + m_i)} \qquad (6)$$

where n_i is the number of observed events in the i-th bin, m_i is the number of Monte Carlo events in the i-th bin, f_i is the average of the theoretical weights f_{ij} of individual Monte Carlo events in the i-th bin:

$$f_i = \frac{1}{m_i} \sum_{j=1}^{m_i} f_{ij}. \qquad (7)$$

The reduced χ^2_{red} is given by $\chi^2/d.o.f = \chi^2/(\text{number of bins} - \text{number of fit parameters}) \sim \chi^2/1024$.

Masses and widths are optimized one at a time in $ln\mathcal{L}$ scans, keeping the masses and widths of the other resonances fixed at the values listed in the Particle Data Group tables [12]. To identify every resonance, 2-dimensional log-likelihood plots are produced. In our initial fits some of the parameters resulted in negligible yields ($< 1\%$). They were kept fixed during the optimization process of subsequent fits. This procedure allowed us to lower the number of free parameters in final fits. In a previous work one overall phase for every resonance was used [9]. In this work, every interference term between two final states has instead been fitted separately with its own phase for every amplitude. We found that reducing the number of phases arbitrarily caused fit instability. Contributions with spin projection $\lambda = 0$ are found to be dominant for tensors in most cases while $|\lambda| = 2$ contributions are negligibly small. All possible $|\lambda| = 1$ contributions are considered, in addition to $\lambda = 0$, in the subsequent fits.

4. Fit results at 900 MeV/c

As a starting point the following intermediate states have been considered:

$$\begin{aligned}
\bar{p}p &\rightarrow \phi(1020)\pi^0 && (a)\\
&\rightarrow f_2(1275)\pi^0 && (b)\\
&\rightarrow f_0(1500)\pi^0 && (c)\\
&\rightarrow K^{*\pm}(892)K^{\mp} && (d)\\
&\rightarrow K_0^{*\pm}(1430)K^{\mp} && (e)
\end{aligned}$$

In this fit only one scalar at 1500 MeV is included. In the initial fits we do not consider the interferences and we optimize only the coupling constants of every single channel but not their relative phases. With the masses and widths fixed at PDG values the basic fit requires the optimization of 8 parameters, giving $ln\mathcal{L} = -348$, $\chi^2_{red} = 2.014$. To take into account the experimental resolution, the $\phi(1020)$ is fitted with a width of 8 MeV. All branching ratios are relative to the $K^*(890)$ ($\lambda = 0$) so the fit is performed actually with 7 free parameters. We find that amplitudes with $|\lambda| > 1$ optimize to a negligible value and can be excluded from the fit. This result is in agreement with analyses of other annihilation channels [15].

Adding the channel

$$\bar{p}p \rightarrow X_J(1710)\pi^0, J = 0 \qquad (f)$$

with mass and width of $f_0(1710)$ the $ln\mathcal{L}$ decreases to -464 ($\chi^2_{red} = 1.777$), with 8 free parameters. The results of this initial fit shows that there is a dominant contribution of the $K^{*\pm}(890)$ (42%) with respect to the other channels. A peak close to ~ 1300 MeV may indicate also the presence of the $a_2(1320)$. Therefore we introduce the channel

$$\bar{p}p \rightarrow a_2(1320)\pi^0. \qquad (g)$$

A change of 103 in the log-likelihood with the introduction of 2 more parameters is obtained ($ln\mathcal{L} = -567$, $\chi^2_{red} = 1.605$, 10 parameters in total).

A preliminary mass and width scan of the channel (f) with $J = 0$ gives an optimum at $M = 1680$ MeV, $\Gamma = 120$ MeV ($ln\mathcal{L} = -581.$, $\chi^2_{red} = 1.571$). After this optimization the fit looks inadequate (see fig. 5).

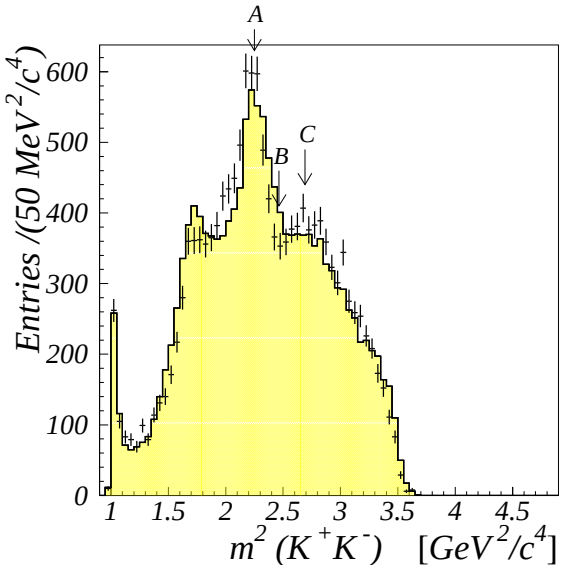

Figure 5. K^+K^- invariant mass projection at 900 MeV/c. The curve is from an initial fit. The arrows indicates a $m(K^+K^-)$ of 1500 (A), 1570 (B), 1640 MeV (C).

Peaks at $\sim$ 1500 and $\sim$ 1640 MeV and a dip at $\sim$ 1570 MeV are not correctly described. The dip may be due to a destructive interference, presumably caused by $f_2'(1525)$. Indeed introducing another tensor with mass and width of $f_2'(1525)$ (channel (h)) in addition to the channels (a)-(f) and allowing interference with $f_0(1500)$ result in a relevant change of the log-likelihood by $\Delta ln\mathcal{L}/\Delta p = 463/4$ where p is the number of additional parameters. The improvement of the fit with respect to the shape of the peak at $\sim$ 1500 MeV is visible (fig. 6) with $\chi^2_{red} = 1.457$ but there are still significant deficiencies.

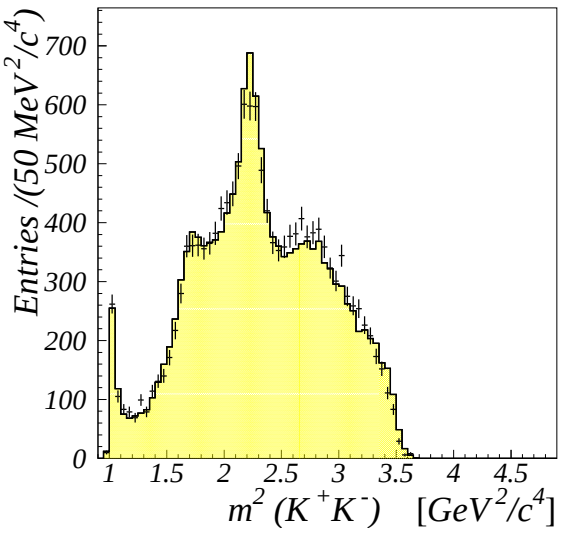

Figure 6. K^+K^- invariant mass projection at 900 MeV/c. The curve is from an improved fit where partial coherence between the $f_0(1500)$, $f_2'(1525)$ and $X_J(1710)$ with $J = 0$ is considered.

To simulate in an approximate way the θ dependence of the charged resonances the amplitudes corresponding to $K^{*+}(890)$ and $K^{*-}(890)$ are multiplied by a factor

$$F(\theta) = 1 + r_1 cos\theta + r_2 cos^2\theta \qquad (8)$$

The parameters r_1, r_2 are fitted separately for each K^{*+}s and K^{*-}s to consider forward-backward asymmetries in their production angles. An improvement of $\Delta ln\mathcal{L}/\Delta p = 579/4$ with the optimization of four more production parameters is obtained.

The optimization of the production process is repeated for the $K_0^{*\pm}(1430)$ with the absolute value of the log-likelihood decreased to -1948 ($\Delta ln\mathcal{L}/\Delta p = 282/4$). Likelihood scans of the resonance parameters yielded a maximum as a function of mass, but no clear maximum as a function of width. This is probably due to the nearness of the $K_0^{*\pm}(1430)$ to the $K^{*\pm}\pi^0$ phase space limit. Spin 0 is found to be preferred over spin

2 by $\Delta ln\mathcal{L} = 153$. Since the results for other resonances are not affected significantly by +/- 50 MeV variations of the $K_0(1430)$ width, we kept the resonance parameters fixed to the PDG values. Tests to see if the $K_2^{*\pm}(1430)$ is also present were not successful.

Intermediate states $\bar{p}p \to X\pi^0, X \to K^+K^-$ are invariant under C-parity therefore the differential cross section is symmetric in θ. Therefore the production process of K^+K^- channels has been tested by multiplying the relative amplitudes by factor

$$F(\theta) = 1 + r_1 cos^2\theta. \quad (9)$$

Improvements of $\Delta ln\mathcal{L}/\Delta p = 70/2$ and $23/2$ fitting 4 more production parameters are obtained for $f_2(1270)$ and $a_2(1320)$, respectively. No significant improvements are obtained for the other channels.

Preliminary spin tests for the channel (f) are performed and $J = 1$ is preferred over $J = 2, 3$ by $\Delta ln\mathcal{L} = 44, 41$, respectively with same number of parameters. $J = 0$ is disfavoured by $\Delta ln\mathcal{L} = 37$ with two parameters less. If $J = 1$ the optimum is reached at $M = 1667 \pm 15$ MeV, $\Gamma = 129 \pm 38$ MeV. Additional spin tests including interference terms with the $K^{*\pm}(890)$ and $K_0^{*\pm}(1430)$ are also performed. These interferences have no effect on spin tests and $J = 1$ is still preferred over $J = 0, 2, 3$.

No significant self-interference of the $K^{*\pm}(890)$ is observed while interference of $K^{*\pm}(890)$ with $K_0^{*\mp}(1430)$ and self-interference of $K_0^{*\mp}(1430)$ gives $\Delta ln\mathcal{L}/\Delta p = 51/2$ and $\Delta ln\mathcal{L}/\Delta p = 28.9/2$, respectively.

Tests to verify also if two resonances in the 1.7 GeV mass range are present were performed. No convincing evidence was obtained. The $K^{*\pm}(892)$ bands cross the diagonal bands at a $m_{K^+K^-}$ mass of $\sim$ 1760 MeV. This makes the observation of any other structure in this mass range difficult.

At lower mass there is an indication of a narrow 2++ state with $M = 1640 \pm 5$ MeV and width of 44 ± 9 MeV (fig. 9). The signal is weak with a yield of 1.9%. However interference with the vector at 1667 MeV yields some significance: adding to the previous fit log-likelihood increases by 34 with six more parameters. $J = 0, 2$ are preferred over $J = 1$ ($\Delta ln\mathcal{L} = 23$). A better optimum in the width is obtained if $J = 2$, but $J = 0$ cannot be excluded here. The fitted mass and width are in accordance are in accordance with those of PDG's resonance candidate $f_2(1640)$ (see table 1).

Spin tests for the channel (f) are performed again and and the results which are shown in fig. 8 confirm that $J = 1$ is preferred over $J = 0, 2, 3$. The vector optimize now at $M = 1700 \pm 15$ MeV and $\Gamma = 129 \pm 38$ MeV.

The results of the optimization and spin tests of $f_2'(1525)$ which is found to be fully coherent with $f_0(1500)$ are shown in fig. 10.

Mass and width scans are done for all the remaining states and the results are given in table 1.

The results of the fits which give $ln\mathcal{L} = -2267$ with 37 decay and 12 production parameters (r_i) are shown in fig. 7. The agreement with the data is satisfactory ($\chi^2_{red} = 1.388$).

Interferences which were tried are summarized in table 2. Those which were considered as significant correspond to a reduction of $ln\mathcal{L} > 3$ per number of additional parameter and are kept in the final fit.

Of these the following have a large coherence coefficient ($|c_\lambda| > 0.7$): $K_0(1430) \times K_0(1430)$, $f_2(1525) \times f_0(1500)(\lambda = 0)$, $f_2(1640) \times (\phi/\rho)_1(1680)(|\lambda| = 0, 1)$, $f_2(1525) \times K_1(890)(|\lambda| = 1)$, $K_1(890) \times f_2(1275)(|\lambda| = 1)$. Although many interferences are not significant, their potential influence on the extracted resonance yields was studied. In general, the effects were found to be only a few percent of the given yields. This was also found when interferences of states with different lambda were admitted.

When different production parameters are allowed for different spin projection λ, as mentioned in Section 3, the yields of resonances are found to change by less than 10% of the values given in Table 1, except for the $f_2(1270)$ where the yield decreases from 8.8 to 7.7% and $a_2(1320)$ where the yield increases from 6.2 to 7.4%. For the sake of transparency such effects are not included in the final yields but taken into account in the error estimate.

Table 1
Fitted masses and widths and yields at 900 MeV/c. Mass and width of a resonance are obtained from 2-dimensional log-likelihood plots. In the fit masses and widths of the other resonances are kept fixed at the values listed in the Particle Data Group tables [12]. Errors are statistical only and correspond to a reduction of $ln\mathcal{L}$ by 0.5. The uncertainties of the yields, including systematic errors from insignificant interferences and from the approximative treatment of the dependence on production angle, are estimated to amount to 15% of the given values, except for the yields of $a_2(1320)$ and $(a/f)(1640)$ where the uncertainty is 30%.

Resonance	Mass (MeV)	Width (MeV)	Yields(%)*	$\Delta(ln\mathcal{L})$**
$K^{*\pm}(892)$	891.9 ± 0.6	56.3 ± 1.7	**44.3**	2527.8
$K_0^*(1430)$	1424 ± 19	PDG	**29.3**	395.3
$\phi(1020)$	1019.3 ± 0.3	< 8.0	2.0	264.9
$f_2(1275)$	1288 ± 9	170 ± 21	**8.8**	44.7
$a_2(1320)$	1324 ± 7	127 ± 25	**6.2**	12.8
$f_0(1500)$	1495 ± 4	121 ± 8	**33.3**	125.5
$f_2'(1525)$	1513 ± 4	76 ± 6	**16.3**	100.0
$(a/f)_2(1640)$	1640 ± 5	44 ± 9	1.9	11.9
$(\phi/\rho)_1(1680)$	1700 ± 8	143 ± 24	7.6	161.3

*In evaluating these branching ratios interferences are omitted. Thus contributions do not add up exactly to 100%. Yields in bold are obtained fitting at PDG'04[12] values for the masses and widths of listed resonances. Remaining yields are obtained at fitted masses and widths and at an experimental width of 8 MeV for the $\phi(1020)$. Replacement of $(\phi/\rho)_1(1680)$ by $\rho_1(1700)$ or $\phi_1(1680)$ at PDG parameters does not affect the yields significantly. **Changes to log-likelihood of the best fit dropping the resonance are obtained re-optimizing the remaining parameters.

	$K_1(890)$	$K_0(1430)$	$\phi_1(1020)$	$f_2(1275)$	$a_2(1320)$	$f_0(1500)$	$f_2(1525)$	$(a/f)_2(1640)$
$K_1(980)$	0.3/2							
$K_0(1430)$	**51./2**	**11.7/1**						
$\phi_1(1020)$								
$f_2(1275)$	**20.1/4**	**7.4/2**						
$a_2(1320)$				0.5/4				
$f_0(1500)$	0.2/2	3.9/2						
$f_2(1525)$	**15.2/4**	1.0/2				**69.9/2**		
$(a/f)_2(1640)$							0.5/4	
$(\phi/\rho)_1(1700)$	7.9/4	**28.9/2**						4.8/4

Table 2
Interferences at 900 MeV/c. Changes to log-likelihood per number of additional parameters are given. Values in bold are the most significant and correspond to a reduction of $ln\mathcal{L} > 3$ per number of additional parameters.

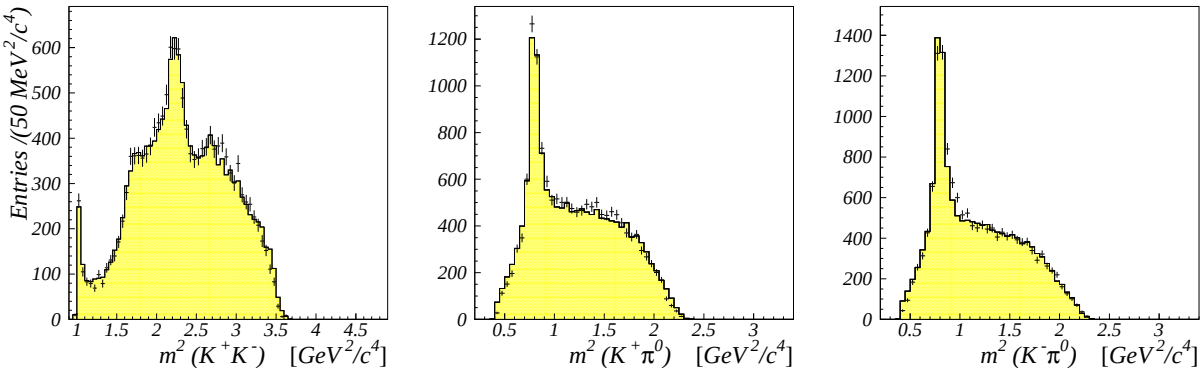

Figure 7. Invariant mass projections at 900 MeV/c. Curves are from the best fit (Table 1).

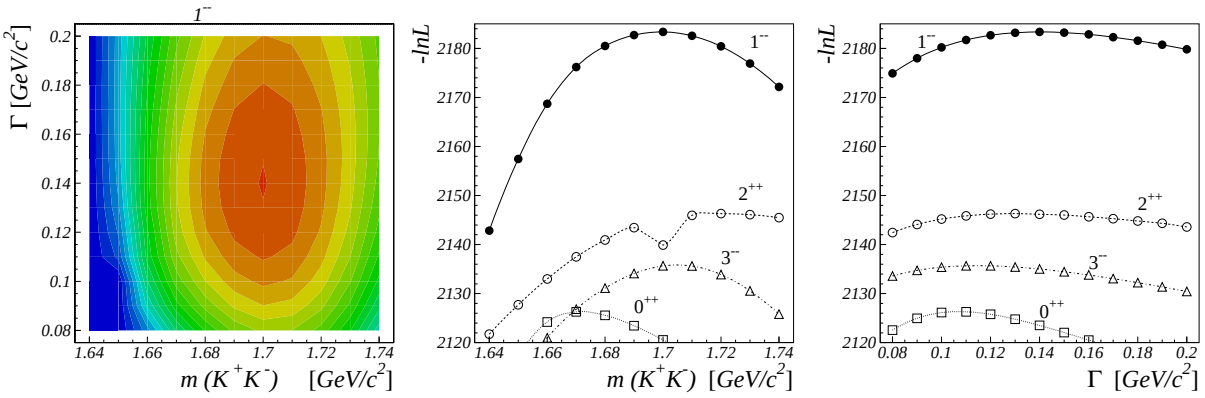

Figure 8. Optimization of the $(\phi/\rho)_1(1680)$ at 900 MeV/c. The optimum is reached at a mass of 1700 ± 8 MeV and width of 143 ± 24 MeV for $J = 1$. $J = 2, 3$ is excluded by a change of at least $37, 48$ respectively in the log-likelihood with the same number of parameters. $J = 0$ is excluded by a change of at least 57 with 2 parameters less.

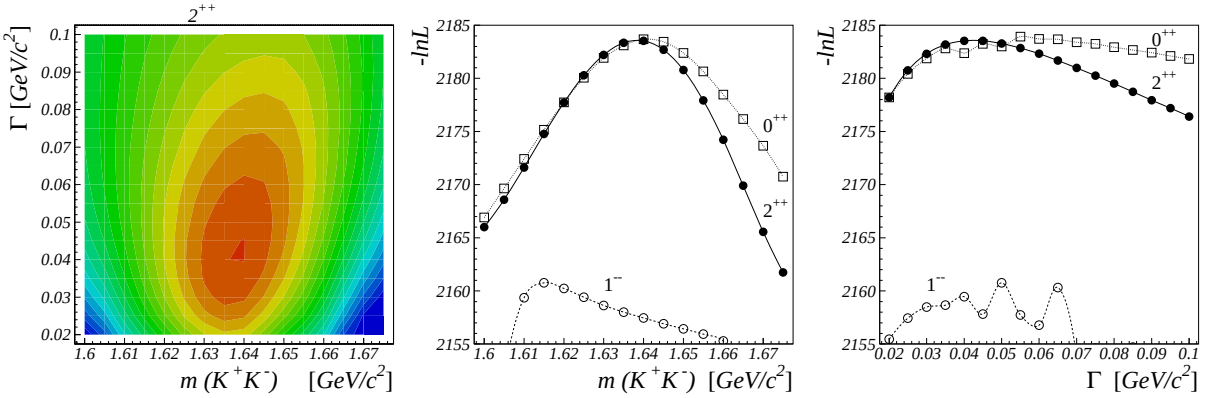

Figure 9. Optimization of $a/f_2(1640)$ at 900 MeV/c. A better optimum as a function of Γ is reached at a mass of 1640 ± 5 MeV and width of 44 ± 9 MeV for $J = 2$ but $J = 0$ cannot be excluded here. $J = 1$ is excluded by a change of at least 23 respectively in the log-likelihood with the same number of parameters.

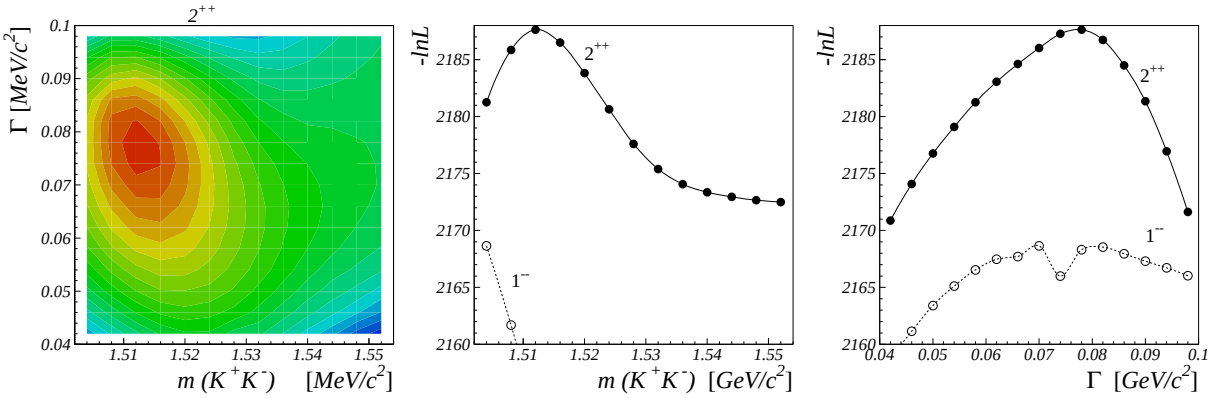

Figure 10. Optimization of $f_2'(1525)$ at 900 MeV/c. The optimum is reached for $J = 2$ and at a mass of 1513 ± 4 MeV and width of 76 ± 6 MeV with 25 decay parameters in total. $J = 0, 1$ is excluded by a change in the log-likelihood of at least $54, 19$ with $23, 25$ parameters, respectively. Points for $J = 0$ are outside of the histogram limits.

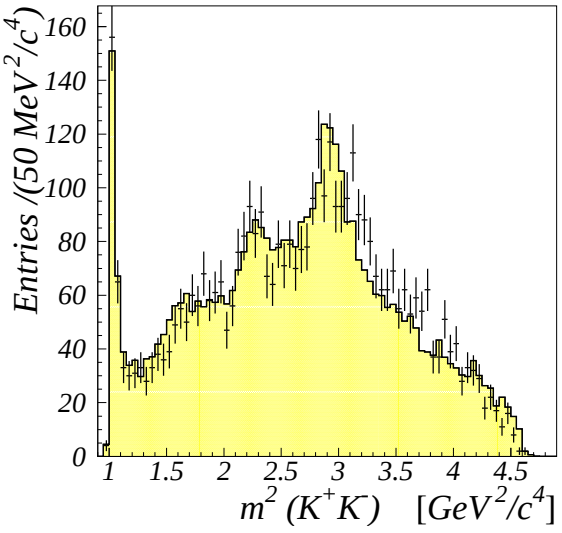

Figure 11. K^+K^- invariant mass projection at 1642 MeV/c. The curve is from a basic fit with a scalar at $M = 1713$ MeV ($\Gamma = 125$ MeV).

5. Fit results at 1642 MeV/c

The channels taken into consideration at 1642 MeV/c for a basic fit are:

$$\begin{aligned}
\bar{p}p &\rightarrow \phi(1020)\pi^0 && (a)\\
&\rightarrow f_2(1275)\pi^0 && (b)\\
&\rightarrow f_0(1500)\pi^0 && (c)\\
&\rightarrow K^{*\pm}(892)K^{\mp} && (d)\\
&\rightarrow K_0^{*\pm}(1430)K^{\mp} && (e)\\
&\rightarrow X_J(1712)\pi^0, J=0 && (f)
\end{aligned}$$

with channel (f) having mass and width of $f_0(1710)$. The basic fit has a log-likelihood of -451.5 and $\chi^2_{red} = 1.608$ with 8 free parameters. Masses and widths are taken form the PDG [12]. The K^+K^- invariant mass projection of this basic fit including the channels (a)-(f) is shown in fig. 11. If we substitute the channel

$$\bar{p}p \rightarrow K_2^{*\pm}(1430)K^{\mp} \qquad (g)$$

instead of $K_0^{*\pm}(1430)$ log-likelihood worsens to $-432.$ with one additional parameter. Furthermore adding $K_2^{*\pm}(1430)$ the improvement in the log-likelihood is not significant and its contribution is negligible so we omit channel (g) from further fits. There is instead a significant improvement when channel

$$\bar{p}p \rightarrow K_1^{*\pm}(1680)K^{\mp} \qquad (h)$$

is included with a log-likelihood of -460.5 and 10 parameters in total. An additional structure around 1920 MeV is visible in the Dalitz plot. Therefore, we include the channel

$$\bar{p}p \rightarrow X_J(1910)\pi^0, J=2 \qquad (i)$$

A resonance in this mass range can be associated with the $f_2(1910)$ and here is confirmed with a $\Delta ln\mathcal{L} = 32.3$, $\chi^2_{red} = 1.532$ with two more additional parameters (if it has spin 2) and a significant contribution (7.4%). Preliminary mass and width scans are performed: for channel (f) mass peaks at ~ 1740 MeV and width at ~ 170 MeV if $J = 0$. We consider also, as at 900 MeV/c, the following channels in addition to (a)-(f),(h),(i):

$$\begin{aligned}
\bar{p}p &\rightarrow f_2'(1525)\pi^0 && (j)\\
\bar{p}p &\rightarrow a_2(1320)\pi^0 && (k)
\end{aligned}$$

We obtain a better fit when $f_2'(1525)$ (channel (j)) is added with a $\Delta ln\mathcal{L}/\Delta p = 9.1/4$. As at lower momentum $f_2'(1525)$ is fully coherent with $f_0(1500)$. After introduction of $f_2'(1525)$, mass and width scans for the $f_0(1500)$ yield good agreement with the accepted resonance parameters (fig. 12). Different spins for the $f_0(1500)$ are rejected (no convergence if $J = 1, 2$). Mass, width and spin tests confirm the presence of $f_2'(1525)$ (see fig. 13). The improvement of the fit when $a_2(1320)$ (channel (k)) is also included is only of $\Delta ln\mathcal{L}/\Delta p =\sim 1.2/2$ and channel (b) ($f_2(1275)$) reproduces almost adequately the Dalitz plot in this mass range.

Excluding $X_J(1740)$ from the fit and optimizing the yields of all other channels the fit deteriorates with a considerable change in the log-likelihood of $\Delta ln\mathcal{L} = -108.5$. This resonance can be possibly formed by an admixture of two states. In order to evaluate this possibility we add another channel in addition to (a)-(f),(h)-(k):

$$\bar{p}p \quad \rightarrow \quad X_J(1680)\pi^0, J = 1 \qquad (l)$$

Re-optimizing the mass and width of channel (f) and (l) an improvement of $\Delta ln\mathcal{L} \sim 3$ is obtained. For channel (l) only $|\lambda| = 1$ amplitude contributes. In contrast to the low momentum case, spin tests yield no significant $ln\mathcal{L}$ distinction of spin 1 and 2 here, both showing similar peaking in the scans. No additional $f_2(1640)$ can be resolved in the $ln\mathcal{L}$ scan, which may be due to the lower statistics. Also a possible contribution of $a_2(1700)$ cannot be excluded (see below).

Amplitudes corresponding to $K^{*\pm}(890)$ and $K_0^{*\pm}(1430)$ are multiplied by factor

$$F(\theta) = 1 + \sum_{i=1,4} r_i cos^i\theta. \qquad (10)$$

The parameters r_i are fitted separately for each $K^{*\pm}$-state. Log-likelihood improves by 40.5 with 16 more parameters. An improvement of 47 in the log-likelihood with 12 more parameters is obtained when amplitudes corresponding to channel (b),(c),(f),(j),(k),(l) are also multiplied by factors

$$F(\theta) = 1 + r_2 cos^2\theta + r_4 cos^4\theta. \qquad (11)$$

No significant improvements are obtained for the remaining channels. Interference between $K_0^{*\pm}(1430)$ and channel (f) ($\Delta ln\mathcal{L}/\Delta p \sim 6.2/2$), between $K_0^{*\pm}(1430)$ and $K_1^{*\pm}(1680)$ ($\Delta ln\mathcal{L}/\Delta p \sim 11.1/2$) and self-interference of $K_1^{*\pm}(890)$ ($\Delta ln\mathcal{L}/\Delta p \sim 4.7/2$) are also present. Interferences which were tried are summarized in table 4. Those which were considered as significant correspond to a reduction of $ln\mathcal{L}$ by > 2 per number of additional parameter, have a large coherence coefficient ($|c_\lambda| > 0.7$) and are kept in the final fit. As at 900 MeV/c many interferences are not significant and their potential influence on the extracted resonance yields were found to be only a few percent of the given yields.

Mass and width optimizations are repeated for all the states and the results are listed in table 3.

Spin test are performed for channel (f) and (i) and the results are shown in fig. 14 and 15. Spin 0 is preferred over spin 2 for the $X_J(1710)$ by $\Delta ln\mathcal{L} = 6$ with one parameter less. Allowing λ dependent production parameters (see above) in the case of $J = 2$ does not improve its likelihood.

The present results on the $f_0(1710)$ are only weakly affected when more resonances from the PDG are added to the model space of Table 2. For an additional $a_2(1700)$ or $\rho(1700)$ no significant change in Likelihood and yields below .5% are obtained and the yield of the $f_0(1710)$ decreases by only .3%. An additional broad $f_0(1770)$, as suggested in an analysis of $\bar{p}p \rightarrow \eta\eta\pi^0$ [15], is not accepted by the fit and a free fit of its parameters yields no optimum in the width.

The best fit is shown in fig. 16 and is obtained fitting 22 decay parameters plus 28 production parameters r_i, with $ln\mathcal{L} = -621.6$ and $\chi^2_{red} = 1.500$.

6. Cross sections

In order to determine the integrated cross section in $\bar{p}p \rightarrow (K^+K^-)\pi^0$ we select $\bar{p}p \rightarrow \pi^+\pi^-$, K^+K^- events and we compare the angular distribution with the measurement of Eisenhandler et al. [13]. The selection of the events into $\pi^+\pi^-$ and K^+K^- final states is carried out using the same procedure that has been used to select $K^+K^-\pi^0$ events. Cuts were performed using the *2-prong* triggers with no photons in the calorimeter. The $d\sigma/d\cos(\theta)(\pi^+\pi^- + K^+K^-)$ is normalized to our data and the results are shown in fig. 17. The total cross sections which are obtained by integration over the full solid angle in our channel ($\bar{p}p \rightarrow \pi^0 X, X \rightarrow K^+K^-$, fig. 18) are of 347 μb and 200 μb at 900 MeV/c and 1642 MeV/c, respectively.

7. Conclusion

At 900 MeV/c a vector state at a mass of 1700 ± 8 MeV and width of 143 ± 17 MeV is observed. It could be identified with the first radial excitation of the $\phi(1020)$, the $\phi(1680)$,

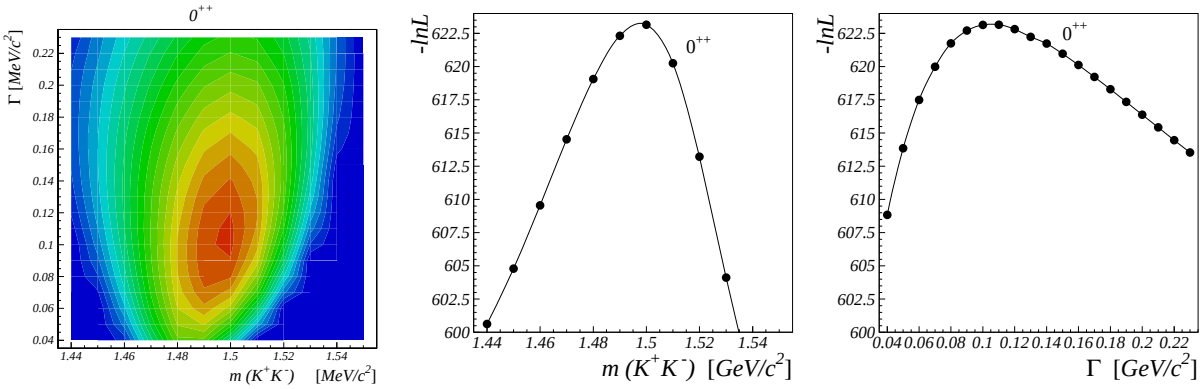

Figure 12. Optimization of $f_0(1500)$ at 1642 MeV/c. The optimum is reached for $J = 0$ and at a mass of 1496 ± 6 MeV and width of 106 ± 14 MeV. If $J = 1, 2$ the fit does not converge.

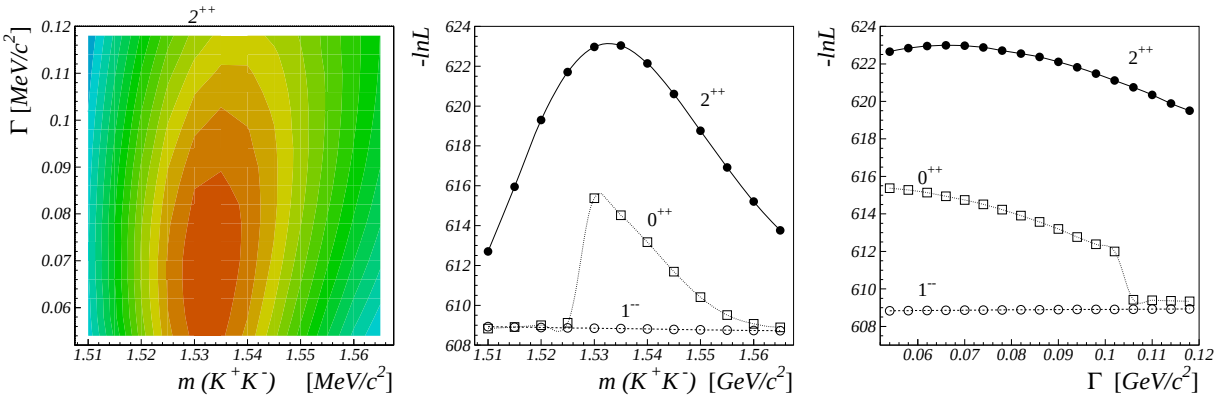

Figure 13. Optimization of $f_2'(1525)$ at 1642 MeV/c. The optimum is reached for $J = 2$ and at a mass of 1533 ± 5 MeV and width of 70 ± 17 MeV. $J = 0, 1$ are excluded by a change of at least $8, 15$, respectively in the log-likelihood with one parameter less for $J = 0$ and with the same number of parameters for $J = 1$.

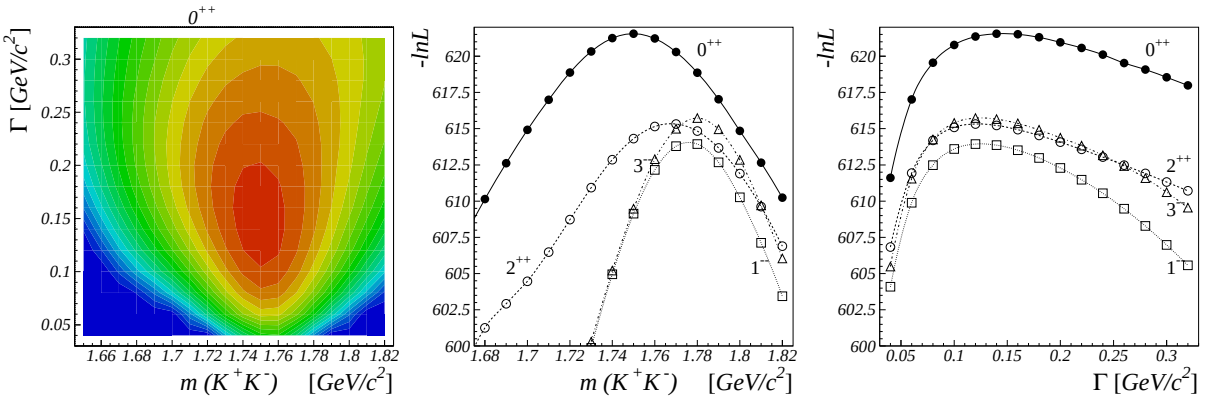

Figure 14. Optimization of $X_J(1710)$ for $J = 0, 2$ at 1642 MeV/c. Optima are reached at a mass of 1750 ± 13 MeV and width of 148 ± 34 MeV if $J = 0$. $J = 0$ is preferred over $J = 1, 2, 3$ by a change of of at least 6 in the log-likelihood with one parameter less.

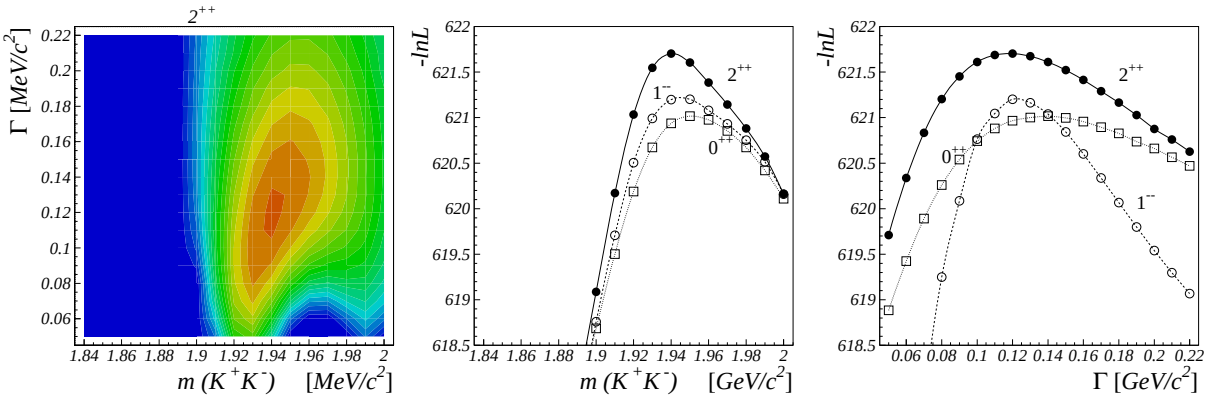

Figure 15. Optimization of $X_J(1910)$ for $J = 0, 1, 2$ at 1642 MeV/c. Optima are reached at a mass of 1941 ± 18 MeV and width of 120 ± 40 MeV if $J = 2$, at a mass of 1947 ± 22 MeV and width of 124 ± 23 MeV if $J = 1$ and at a mass of 1953 ± 26 MeV and width of 143 ± 6 MeV if $J = 0$. $J = 3, 4$ have no optima.

Table 3
Fitted masses and widths and yields at 1642 MeV/c. Mass and width of a resonance are obtained from its 2-dimensional log-likelihood plot. During the fit masses and widths of the other resonances are kept fixed at the values listed in the Particle Data Group tables [12]. Errors are statistical only and correspond to a reduction of $ln\mathcal{L}$ by 0.5. The estimated errors of the yields, including systematic errors (cf. Table 1), amount to up to 20% of the given values.

Resonance	Mass (MeV)	Width (MeV)	Yields(%)*	$\Delta(ln\mathcal{L})$**
$K^{*\pm}(892)$	897.1 ± 1.5	50.9 ± 1.7	**24.3**	388.9
$K_0^*(1430)$	PDG	PDG	**23.7**	120.0
$K_1^*(1680)$	PDG	PDG	**1.4**	16.6
$\phi(1020)$	1019.1 ± 0.5	< 9	4.8	209.6
$f_2(1275)$	1262 ± 10	143 ± 25	**6.4**	48.5
$a_2(1320)$	1340 ± 14	88 ± 31	**2.5**	8.4
$f_0(1500)$	1496 ± 6	106 ± 14	**17.1**	39.6
$f_2'(1525)$	1533 ± 5	70 ± 17	**10.5**	12.9
$X_J(1680)$,$J = 1$	1678 ± 7	99 ± 40	**15.5**	15.3
$f_0(1710)$	1750 ± 13	148 ± 34	5.2	56.9
$X_J(1910)$,$J = 2$	1941 ± 18	120 ± 40	**3.3**	5.3

*In evaluating this branching ratios interferences are omitted. Thus contributions do not add up exactly to 100%. Yields in bold are obtained fitting at PDG'04 [12] values with $X_J(1680)$ and $X_J(1910)$ identified as $\phi_1(1680)$ and $f_2(1910)$, respectively. Remaining yields are obtained at fitted masses and widths with $\Gamma(\phi(1020)) = 9$ MeV. Replacement of the $f_0(1710)$ resonance parameters by the PDG values leads to a slightly different yield (5.9%). ** Changes to log-likelihood of the best fit dropping the resonance are obtained re-optimizing the remaining parameters.

	$K_1(890)$	$K_0(1430)$	$K_1^*(1680)$	$\phi_1(1020)$	$f_2(1275)$	$a_2(1320)$	$f_0(1500)$	$f_2(1525)$	$(\phi/\rho)_1(1680)$	$f_0(1710)$
$K_1(980)$	**4.7/2**									
$K_0(1430)$	1.0/2	0.0								
$K_1^*(1680)$		**11.1/2**								
$\phi_1(1020)$										
$f_2(1275)$	5.3/4	2.7/2								
$a_2(1320)$					0.0					
$f_0(1500)$	0.3/2	1.4/2								
$f_2(1525)$	0.05/2	0.2/2					**9.1/2**			
$(\phi/\rho)_1(1680)$	1.6/5	0.0						0.0		
$f_0(1710)$	0.9/2	**6.2/2**						2.1/2	0.0	
$X_2(1910)$		2.7/2								3.3/2

Table 4
Interferences at 1642 MeV/c. Changes to log-likelihood per number of additional parameters are given. Values in bold are the most significant and correspond to a reduction of $ln\mathcal{L} > 2$ per number of additional parameters.

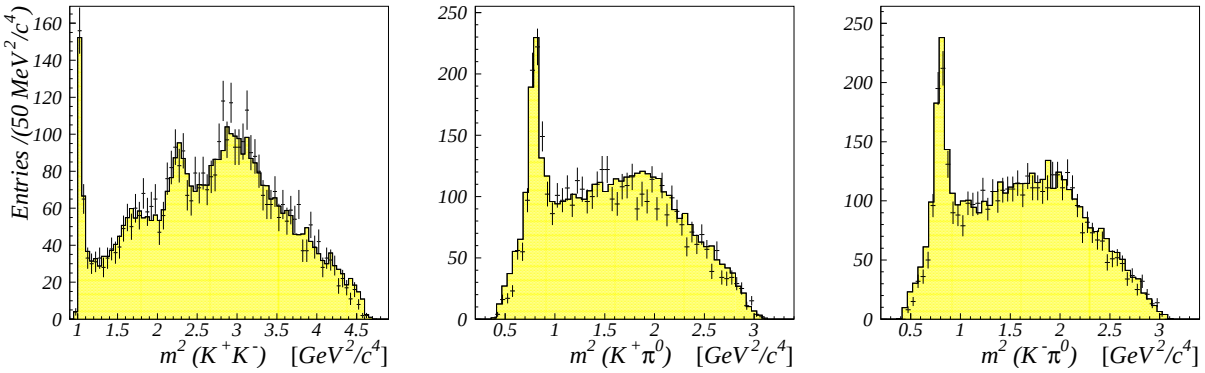

Figure 16. Mass projections at 1642 MeV/c. Curves are from the best fit.

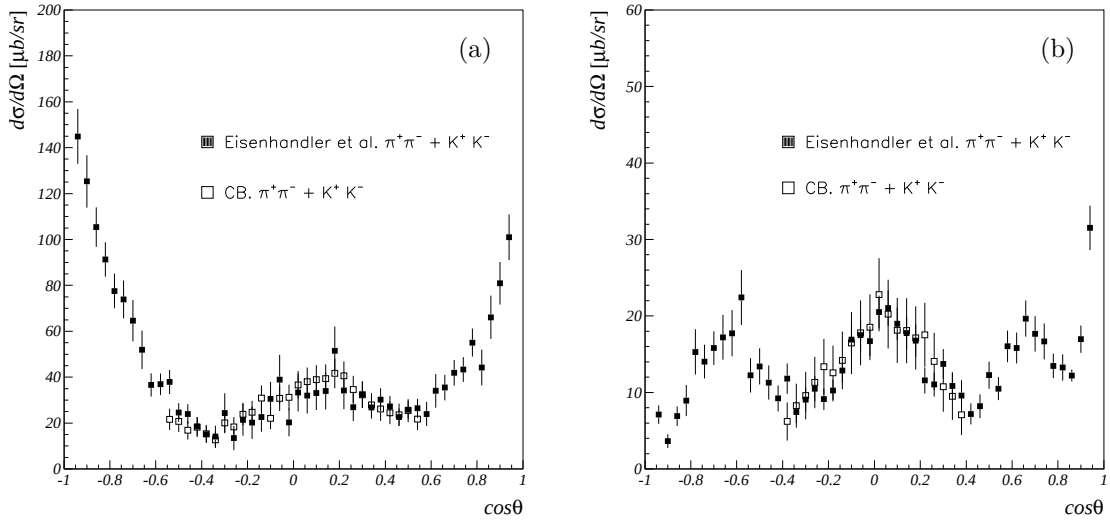

Figure 17. Differential cross sections for $\bar{p}p \to \pi^+\pi^- + K^+K^-$ states at 900 MeV/c (a) and at 1642 MeV/c (b). Because of detector acceptance the normalization to Crystal Barrel data is performed in the (a) $|cos\theta| < 0.58$ and (b) $|cos\theta| < 0.42$ range.

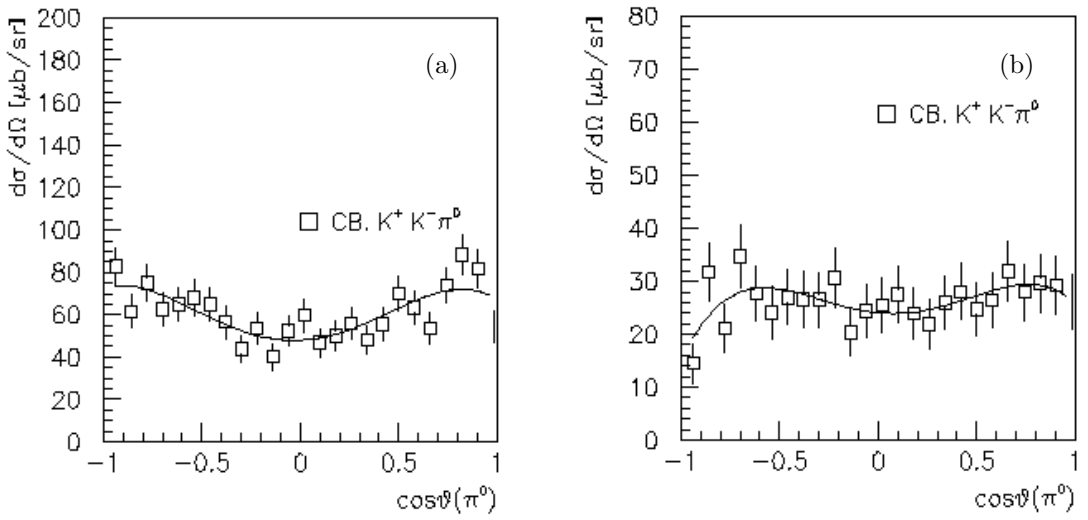

Figure 18. Differential cross sections for $\bar{p}p \to \pi^0 X, X \to K^+K^-$ at 900 MeV/c (a) and at 1642 MeV/c (b).

but because of isospin ambiguity, an eventual mixture with the $\rho_1(1700)$ cannot be excluded. There is also some supportive evidence of a narrow tensor with a mass of 1640 ± 5 MeV and width of 44 ± 9 MeV. This resonance is possibly the $f_2(1640)$ previously observed in the analysis of the data from the MARK III experiment in $J/\psi \to \gamma(\pi^+\pi^-\pi^+\pi^-)$ [14].

The results at 1642 MeV/c are consistent with those at 900 MeV/c. In general the resonance parameters and spins deduced from the present partial wave analyses at both incoming momenta agree reasonably with PDG parameters. However, the spin tests for the state at 1680 MeV could not distinguish J=1 and 2 and an $f_2(1640)$ could not be resolved here, which may be due to the lower statistics. K^+K^- resonances with allowed quantum numbers $J^{PC} = 0^{++}, 1^{--}, 2^{++}$,... that were tried but not required by the fits include $f_0(1370)$, $\omega(1420)$, $\rho(1450)$, $f_2(1565)$, $a_0(1450)$ and $\rho_3(1690)$.

At 1642 MeV/c two other resonances are observed. Mass and widths of the first state are at $M = 1750 \pm 13$ MeV and $\Gamma = 148 \pm 34$ MeV, which is in reasonable agreement with the resonance parameters of the $f_0(1710)$ [12]. Its yield is not as large as that of the $f_0(1500)$. $J^{PC} = 0^{++}$ is preferred over $1^{--}, 2^{++}$ and 3^{--}. Mass optima if $J = 3$ are at least 3 standard deviations higher than the mass of $\rho_3(1690)$ which is therefore excluded. It is found that possible contributions from $\rho_1(1700)$ or $a_2(1700)$ affect the yield from this state only weakly probably because the $X(1680)$ in our fit in our fit covers these to a large extent.

Mass of the second state $M = 1941 \pm 18$ MeV and $\Gamma = 120 \pm 40$ MeV if $J^{PC} = 2^{++}$ are in line with the $f_2(1910)$ observed by GAMS [16], VES [17], WA102 [18]. However, a clear distinction from $f_2(1950)$, with a suggested [12] width of 475 MeV, is not possible here.

REFERENCES

1. I. Uman, Ph.D. thesis University of Munich (2001). (http://www.zup.physik.uni-muenchen.de/)
2. I. Uman [Crystal Barrel Collaboration], Nucl. Phys. A **692**, 302 (2001).
3. I. Uman and O. Kortner, CB-Note 341 (1998).

4. H. Koch, U Kurilla, K. Peters and M. Ratajzcak, CB-Note 343 (1999).
5. M. Heinzelmann, CB-Note 328 (1998).
6. N. Hessey, CB-Note 199 (1992).
7. M. Benayoun et al, CB-Note 280 (1995).
8. GEANT 3.21, CERN Program Library W5013 (1994).
9. A. Abele *et al.* [Crystal Barrel Collaboration], Eur. Phys. J. C **8**, 67 (1999).
10. J. Adomeit *et al.* [Crystal Barrel Collaboration], Z. Phys. C **71**, 227 (1996).
11. O. Kortner and C. Zupancic, Nucl. Instrum. Meth. A **503**, 625 (2003).
12. S. Eidelman *et al.* [Particle Data Group], Phys. Lett. B **592**, 1 (2004).
13. E. Eisenhandler *et al.*, Nucl. Phys. B **96**, 109 (1975).
14. D. V. Bugg, I. Scott, B. S. Zou, V. V. Anisovich, A. V. Sarantsev, T. H. Burnett and S. Sutlief, Phys. Lett. B **353**, 378 (1995).
15. A. V. Anisovich *et al.*, Phys. Lett. B **449**, 154 (1999).
16. D. Alde *et al.* [IHEP-IISN-LANL-LAPP-TSUIHEP Collaboration], Phys. Lett. B **241**, 600 (1990).
17. S. I. Bityukov *et al.*, Z. Phys. C **54**, 367 (1992).
18. D. Barberis *et al.* [WA102 Collaboration], Phys. Lett. B **471**, 429 (2000) [arXiv:hep-ex/9911041].
19. A. V. Anisovich *et al.*, Phys. Lett. B **491**, 47 (2000).